ISSN: 2476-6909; Modares. Mech. Eng. 2027;27(04):339-349.

Modares Mechanical Engineering

DOI: 10.48311/mme.2026.123268.83099
journal homepage: mme.modares.ac.ir

A Systematic Approach to the Design, Optimization, and Fabrication of a Robotic Knee Exoskeleton for Post-Total Knee Arthroplasty Rehabilitation

Raed Abdulameer Mahmood Alalwani[1], Ali Selk Ghafari[2*]

[1] Sharif University of Technology International Campus, Kish Island, Iran, Alfurat Al-Awsat Technical University, Alkufa, Iraq
[2] Sharif University of Technology International Campus, Kish Island, Iran

ARTICLE INFO

Article Type
Original Research

Article History
Received: August 29, 2026
Revised: October 11, 2026
Accepted: October 17, 2026
ePublished: November 14, 2026

ABSTRACT

Rehabilitation post-total knee arthroplasty (TKA) demands intensive physical therapy to restore joint functionality, and prevent joint stiffness. Conventional manual physiotherapy is labor-intensive and costly, while multi-joint whole-leg exoskeletons introduce excessive complexity, high mass, and protracted fitting times ill-suited for isolated joint recovery. This paper presents a systematic framework encompassing the design, finite element analysis driven optimization, and fabrication of a single-degree-of-freedom robotic knee exoskeleton specifically intended for post-TKA rehabilitation. Key design features, including sagittal-plane flexion/extension, joint alignment compensation, low distal inertia, and state-based impedance control, were distilled from a comprehensive synthesis of lower-limb rehabilitation robotics literature. Coupled finite element modeling and Sobol-based global sensitivity analysis revealed that the link thickness and cross-sectional area emerged as the main factor controlling peak stress and deformation. The multi-objective optimization strategy successfully decreased the peak von Mises stress under dynamic loading by 13.2%, attaining 143.9 MPa. In addition, structural deflection was reduced by 27% to 0.62 mm, and yielding the fatigue safety factor of 1.67 with an infinite operational life cycle. Furthermore, cuff-limb interaction forces were reduced by 30% to 44.3 N, effectively mitigating the risk of soft-tissue trauma. The final prototype achieved a total mass of 2.8 kg with a more proximal center of mass, substantially reducing rotational inertia and passive gravitational torque. The proposed prototype provides an optimized, lightweight robotic framework establishing the structural and mechatronic foundation required for subsequent clinical evaluation of progressive post-TKA knee mobilization.

Keywords: Total Knee Arthroplasty, Robotic Exoskeleton, Design, Optimization, Rehabilitation

How to cite this article
Abdulameer Mahmood Alalwani R, Selk Ghafari A, A Systematic Approach to the Design, Optimization, and Fabrication of a Robotic Knee Exoskeleton for Post-TKA Rehabilitation, Modares Mechanical Engineering; 2027;27(04):339-349.

*Corresponding author's email: a_selkghafari@sharif.edu
*Corresponding ORCID ID: 0000-0003-0643-6588

Copyright© 2027, TMU Press. This open-access article is published under the terms of the Creative Commons Attribution-NonCommercial 4.0 International License which permits Share (copy and redistribute the material in any medium or format) and Adapt (remix, transform, and build upon the material) under the Attribution-NonCommercial terms.

شاپا: ۶۹۰۹-۲۴۷۶؛ مهندسی مکانیک مدرس. ۳۴۹-۳۳۹:(۰۴)۲۷؛۱۴۰۶

مهندسی مکانیک مدرس

DOI: 10.48311/mme.2026.123268.83099

صفحه اصلی مجله: mme.modares.ac.ir

رویکرد سیستماتیک در طراحی، بهینه سازی و ساخت یک ربات پوشیدنی برای توانبخشی پس از عمل جراحی تعویض کامل مفصل زانو

رائد عبدالامیر محمود العلوانی[۱]، علی سلک غفاری[۲]*

[۱] دانشگاه صنعتی شریف- پردیس بین الملل کیش، جزیره کیش، ایران، دانشگاه صنعتی فرات الاوسط، فرات، عراق

[۲] دانشگاه صنعتی شریف- پردیس بین الملل کیش، جزیره کیش، ایران

اطلاعات مقاله

نوع مقاله

مقاله پژوهشی

تاریخچه مقاله

دریافت: ۱۴۰۵/۰۶/۰۷

بازنگری: ۱۴۰۵/۰۷/۱۹

پذیرش: ۱۴۰۵/۰۷/۲۵

ارائه آنلاین: ۱۴۰۵/۰۸/۲۳

چکیده

لازمه بازیابی دامنه حرکتی، تقویت قدرت عضلانی و پیشگیری از خشکی و فیبروز مفصلی انجام توانبخشی منسجم پس از تعویض کامل مفصل زانو می‌باشد. روش‌های سنتی فیزیوتراپی پرهزینه و زمان‌بر بوده و استفاده از روبات‌های پوشیدنی چندمفصله بدلیل سنگینی و زمان‌بر بودن تنظیمات اولیه، برای توانبخشی زانو مناسب نیستند. هدف از این پژوهش، ارائه چارچوبی سیستماتیک برای بهینه‌سازی طراحی یک روبات یک‌درجه‌آزادی برای توانبخشی زانو است. ویژگیهای کلیدی برای طراحی، با بررسی جامع ادبیات روبات‌های توانبخشی اندام تحتانی در صفحه ساجیتال استخراج شد. بهینه‌سازی اجزای محدود مدل مکانیکی روبات و تحلیل حساسیت شاخص‌های سوبول نشان داد که ضخامت و سطح مقطع بازوی روبات، به ترتیب مهم‌ترین متغیرهای موثر بر تنش بیشینه و تغییرشکل سازه‌ای می‌باشند. با بهینه‌سازی چندمتغیره تحت بارگذاری دینامیکی، تنش ون‌مایسز با کاهش ۱۳.۲٪ به مقدار ۱۴۳.۹ مگاپاسکال ثبت شد که ضریب اطمینان در برابر بارگذاری خستگی ۱.۶۷ و عمر بینهایت را فراهم می‌نماید. همچنین بیشینه تغییرشکل سازه‌ای با ۲۷٪ کاهش به ۰.۶۲ میلی‌متر بدست آمد. همچنین با کاهش ۳۰٪ نیروی برهم‌کنش در محل اتصال روبات با اندام به ۴۴.۳ نیوتن، خطر آسیب به بافت نرم نیز کاهش می‌یابد. علاوه براین، پس از بهینه‌سازی، جرم کل به ۲.۸ کیلوگرم کاهش و با جابجایی مرکز جرم روبات، ممان اینرسی جرمی و گشتاور گرانشی غیرفعال نیز کاهش یافتند. نمونه بهینه‌سازی‌شده می‌تواند بستر روباتیکی کارآمدی را برای ارزیابی‌های بالینی آتی و بررسی اثربخشی برنامه‌های تدریجی بهبود دامنه حرکتی زانو پس از جراحی تعویض کامل مفصل زانو فراهم آورد.

کلیدواژه‌ها: تعویض کامل مفصل زانو، ربات پوشیدنی، طراحی، بهینه سازی، توانبخشی

نحوه ارجاع به این مقاله

عبدالامیر محمود الالوانی رائد، سلک غفاری علی، رویکرد سیستماتیک در طراحی، بهینه سازی و ساخت ربات پوشیدنی برای توانبخشی پس از عمل جراحی تعویض کامل مفصل زانو، مهندسی مکانیک مدرس. ۳۴۹-۳۳۹:(۰۴)۲۷؛۱۴۰۶

*پست الکترونیکی نویسنده عهده‌دار مکاتبات: a_selkghafari@sharif.edu

*شناسه ارکید نویسنده عهده‌دار مکاتبات: ۰۰۰۰-۰۰۰۳-۰۶۴۳-۶۵۸۸

Copyright© 2027, TMU Press. This open-access article is published under the terms of the Creative Commons Attribution-NonCommercial 4.0 International License which permits Share (copy and redistribute the material in any medium or format) and Adapt (remix, transform, and build upon the material) under the Attribution-NonCommercial terms.

1- Introduction

TKA has become widely popular worldwide in the past twenty years for the treatment of various knee pathologies, including osteoarthritis [1]. Post-TKA rehabilitation requires progressive physical therapy to restore joint functionality and achieving symmetric gait. Traditional rehabilitation methods are labor intensive, often necessitating multiple therapists to manually assist the patient's limbs, which significantly increases clinical costs and staffing demands. The rapid advancement of sophisticated robotic systems, coupled with the growing convergence of human-robot interaction paradigms, has engendered substantial opportunities for deploying these technologies within healthcare ecosystems. Consequently, the integration of such systems with intelligent control architectures presents a transformative potential for personalized rehabilitation and assistive applications. To contextualize the trajectory of research in this domain, a concise synthesis of the historical benefits and limitations associated with robotic-assisted exoskeletal rehabilitation systems is warranted.

The genesis of mechanized rehabilitation can be traced to the Continuous Passive Motion mechanism (CPM), first proposed in 1983 [2], which employed a two-bar linkage to progressively enhance the ROM in the ankle, knee, and hip joints within the sagittal plane. However, clinical investigations evaluating CPM efficacy have demonstrated that its passive operational paradigm yields no significant reconstructive benefit for patients undergoing TKA [3–4]. The cumulative evidence from medical literature underscores the necessity for active patient engagement in the rehabilitation process to optimize recovery outcomes for TKA patients [5].

Since the late 1980s, various lower-limb exoskeletons have been developed to provide controlled assistance for gait rehabilitation in patients with spinal cord injury (SCI) and stroke. Notable systems include HAL, which integrates electric actuation and myoelectric control [6]; Ekso GT, which combines electrical actuation with functional electrical stimulation [7–9]; REX, which employs multi-joint actuation to enable assisted ambulation [10]; ReWalk, approved for home use in 2015 [11–12]; Indego, which supports walking and postural transitions [13]; and SuitX Phoenix, designed for standing stability and assisted walking [14]. Although the primary focus of these systems remains neurological rehabilitation rather than the specific demands of post-TKA rehabilitation. Moreover, a critical limitation across these systems is their simple hinge form of the knee joint. Physiologically, knee flexion/extension is inextricably linked to anterior/posterior tibial translation, involving concomitant sliding and rotational kinematics between the femur and tibia.

A select number of next-generation robotic exoskeletons have addressed this shortcoming, with notable contributions reported in [15–19]. Specifically, the AssistOn-Knee system proposed in [15] integrates a lightweight knee brace incorporating a Schmidt coupling and optical incremental encoder, actuated by a series elastic actuator (SEA) to compensate for kinematic discrepancies during motion, with a high-gain position controller for torque computation. The two model-based torque control approaches proposed for the Sharif lower-limb exoskeleton equipped with SEA in [16], based on velocity and current commands, demonstrate excellent torque tracking accuracy, effectively addressing this issue. The self-adjusting mechanism in [17] employs an encoder-based tracking system integrated with a gait-phase predictive controller. An alternative strategy described in [18] utilizes a pneumatic soft-actuated mechanism to emulate tibiofemoral articulation. A lightweight active knee-ankle-foot orthosis proposed in [19] features a back-drivable knee actuator with a finite-state-machine-based trajectory generator and position-based impedance control. A comprehensive review of the past several decades of research reveals that the predominant focus in assistive exoskeleton development has been the design of compliant mechanical systems and robust control strategies to ensure safe human-robot interaction [20]. Moreover, the literature indicates that the design of exoskeletal assistive devices is particularly challenging owing to the possibility of incorporating programmable actuation to facilitate knee and hip joint motion during gait cycles [21].

Despite advances in lower-extremity exoskeletons, the specific biocompatibility requirements of post-TKA rehabilitation warrant further investigation. These requirements include progressively restoring full knee extension to minimize the risk of flexion contractures through active patient participation. In this context, assist-as-needed (AAN) control may be an approach to complement CPM by accommodating the patient's voluntary effort. Additional design considerations include minimizing localized pressure near healing surgical incisions. Reducing distal limb mass and rotational inertia through utilizing lightweight structural materials and appropriate actuator placement, are other issues should be considered. Furthermore, minimizing discrepancies between the joint axis of the exoskeleton and the knee's anatomical instantaneous center of rotation (ICR) mitigates parasitic interface forces and shear. Although dedicated robotic systems specifically addressing post-TKA rehabilitation remain insufficiently characterized in the literature. Furthermore, the lack of well-established design guidance linking biomechanical requirements, and into engineering specifications challenging. These gaps motivate the development of a systematic engineering approach to the design, optimization, and fabrication of an efficient exoskeleton for post-TKA rehabilitation.

To address these limitations, this paper presents a systematic framework for the design, finite element optimization, and experimental prototyping of a dedicated one-degree-of-freedom (DOF) robotic knee exoskeleton tailored for post-TKA rehabilitation. First, we synthesize critical design features and biomechanical requirements from existing lower-limb robotic rehabilitation systems to establish core kinematic, kinetic, and safety parameters for isolated sagittal knee assistance. Next, we implement a multi-objective finite element method (FEM) and global sensitivity analysis (Sobol indices) to optimize the structural geometry of the exoskeleton linkage in Al 7075-T6, directly mitigating peak dynamic stresses, controlling compliance, reducing cuff-limb interaction forces, and shifting the device's center of mass (CoM) proximally to minimize distal rotational inertia. Finally, we detail the physical fabrication and mechatronic implementation of the lightweight prototype, integrating control paradigms to bridge the continuum from early CPM to active-assisted overground gait stabilization.

2- Materials and Methods

2-1- Classifications of Lower-Extremity Rehabilitation Robotics

Robotic lower-limb devices can be categorized based on their mechanical architecture and therapeutic approach. in the first category exoskeletal robots are integrated with a treadmill or body-weight support (BWS) to guide limb trajectories during ambulation. Examples of this category include the Lokomat [22], LokoHelp [23], ALEX [24], and LOPES [25]. A second category encompasses foot-plate-based trainers, which the patient's feet are positioned on independently driven footplates to simulate both stance and swing trajectories, as seen in the Gangtrainer GT I [26], HapticWalker [27], and GaitMaster5 [28]. Furthermore, overground gait trainers comprise both mobile platforms, such as the KineAssist [29] and Walk Trainer [30], and wearable orthotic suits, including the ReWalk [12] and HAL [6, 31–32], which enable unrestricted overground ambulation. Finally, stationary and joint-specific systems are targeted robotic devices designed to mobilize individual joints without facilitating overground walking; notable examples include the MotionMaker [33], Rutgers Ankle [34], and the Active Knee Rehabilitation Orthotic Device (AKROD) [35].

2-2- Extracting of Key Design Features for Robotic Knee Exoskeletons

From a kinematic perspective, human knee articulation in the sagittal plane spans from full extension, 0°, to approximately 60° during level walking, reaching 120°–135° in deep flexion; post-TKA rehabilitation

thus mandates terminal extension to prevent flexion contractures alongside progressive flexion recovery [36]. Unlike rigid single-axis hinges, the anatomical knee follows a polycentric ICR during flexion, which necessitates the incorporation of a polycentric or ICR self-aligning mechanism, passive degrees of freedom, and adjustable thigh/shank linkages to mitigate joint misalignment and tissue shear [37–38].

Regarding actuation and mass allocation, distal segment mass significantly elevates metabolic cost [39]; consequently, offboard or proximal actuation paired with flexible Bowden-cable transmissions [40], effectively reduces on-limb inertia while preserving torque fidelity.

To safeguard against joint overloading, mechanical compliance is realized via SEAs [41] or controllable fluid dampers utilizing electrorheological [35] or magnetorheological [42] principles. Peak torque requirements dictate approximately 0.25 Nm/kg for swing-phase flexion assistance and 0.5–1.0 Nm/kg for stance-phase extension and sit-to-stand maneuvers [43–44]. Notably, optimized exoskeletal torque profiles diverge substantially from biological trajectories, with stance-phase extension stabilizing the limb and swing-phase flexion facilitating foot clearance.

The control architecture combines state-based impedance modulation, employing virtual spring stiffness during stance to prevent buckling and virtual damping during terminal swing to mitigate hyperextension, with an AAN paradigm [24, 45–46], that dynamically adjusts output based on surface electromyography (sEMG) or torque feedback to encourage active patient participation. Clinically, the system addresses the full continuum of post-TKA recovery through three distinct operation modes: (1) CPM for early ROM mobilization, (2) active-assisted strengthening and resistance training, and (3) stance stabilization during overground walking, thereby providing a unified platform that progresses from passive immobilization to functional ambulatory support.

2-3- Single-Joint vs. Multi-Joint Trade-Offs and Architectural Synthesis

Empirical comparisons of single-joint, two-joint, and whole-leg exoskeleton configurations demonstrate a clear hierarchy of metabolic benefit relative to mechanical complexity [47]. Among one-DOF systems, ankle-only assistance produces the greatest single-joint metabolic saving (approximately 30%) during level walking; however, this advantage is offset by a substantial distal mass penalty and reduced comfort at elevated push-off torques. Hip-only assistance achieves a metabolic reduction of approximately 26% through proximal actuation, yet necessitates extensive pelvic bracing. In contrast, knee-only assistance yields the lowest metabolic benefit (approximately 13%), although it offers distinct advantage in a lightweight targeted joint rehabilitation, and superior patient comfort. Expanding to multi-joint architectures, the hip-ankle (2-DOF) configuration achieves a ~42% reduction by capturing the majority of walking power, albeit with complex coupling between non-adjacent joints. At the upper extreme, whole-leg (3-DOF) systems deliver maximum metabolic unloading (~50%) at the cost of considerable bulk, high mechanical complexity, and a substantial system mass, approximately 13.5 kg for emulator-based implementations.

This hierarchy is further contextualized by the indirect assistance phenomenon: whole-leg assistance, 50%, falls appreciably short of the linear summation of individual single-joint contributions (13 % + 26 % + 30 % = 69 %), indicating that single-joint assistance inherently unloads muscles spanning adjacent unassisted joints via biarticular coupling and compensatory kinematic adaptations, for example, knee and ankle assistance have been shown to reduce gluteus maximus activation during gait. Consequently, for isolated knee pathologies such as post-TKA rehabilitation, a one-DOF knee exoskeleton remains the most clinically appropriate choice.

Table 1 Summary Matrix of Design Specifications for Post-TKA Exoskeletons

Category	Specification	Post-TKA Robotic Design Target
Kinematics	Degrees of Freedom	1 active DOF (Sagittal Flexion/Extension)
	Angular ROM	0° to 120° with hardware & software limiters
	Axis Compatibility	Polycentric / ICR self-aligning mechanism
Mechanical	Mass Allocation	< 3.5 kg on limb (remote or proximal actuator
	Actuator Selection	Series Elastic Actuator (SEA) / Bowden-cable drive
	Peak Torque Capability	0.3 - 0.5 Nm/kg (stance ext.), ~0.25 Nm/kg (flex.)
Control & Safety	Control Scheme	State-based impedance (stance spring, swing damper)
	Interaction Mode	AAN with sEMG / torque feedback
Clinical Use	Operation Modes	- Continuous Passive Motion (Early ROM mobilization) - Active-Assisted Strengthening & Resistance - Stance Stabilization during Overground Walking

It provides active strengthening of the quadriceps and hamstrings, and stance-phase support, while avoiding the excessive weight, and prolonged fitting requirements associated with multi-joint systems. The essential design specifications for a knee exoskeleton intended for post-TKA rehabilitation are systematically summarized in Table 1.

2-4- Initial Conceptual Design

In contrast to laboratory-based systems with complex multi-joint mechanisms and lengthy fitting procedures, the proposed device should be lightweight and relatively simple, making it suitable for practical, unsupervised home use. Joint-axis misalignment in wearable exoskeletons may arise from four primary sources. These sources are kinematic differences between the device and the anatomical joint, migration of the ICR, initial anatomical offsets associated with soft-tissue coverage, and relative motion between the limb and the device during operation. Recommended approaches to mitigate these effects include careful manual alignment during donning, utilizing compliant elements at the brace, frame, or joint level, and the use of additional kinematic degrees of freedom, such as RRP, RPP, or RRR mechanisms [48-53]. Although kinematic redundancy can accommodate greater relative motion, it generally increases device mass, volume, and mechanical complexity [49]. Because the human knee does not behave as an ideal single-axis hinge, complete elimination of anatomical–mechanical axis mismatch cannot be expected [50]. In contrast, careful anthropometric fitting combined with the compliance of the human soft tissue and intermediate 10 mm EVA padding provides a simpler approach to suppress resulting parasitic anterior-posterior (A-P) shear and maintain a lightweight and compact architecture [51, 53]. Accordingly, a single-axis revolute hinge was selected for the proposed 1-DOF knee exoskeleton as an engineering simplification, consistent with the approach adopted in most previously developed exoskeletons [12, 31–32] and rehabilitation devices [22–25]. This level of kinematic incompatibility is deemed clinically acceptable for the targeted post-TKA population, particularly when balanced against the substantial benefits of reduced system mass and enhanced user autonomy.

To minimize residual kinematic incompatibility, prior to each experimental session, the exoskeleton should be adjusted by an experienced physiotherapist using established clinical alignment principles. In this procedure, the lateral femoral epicondyle was identified by palpation as an anatomical reference to estimate the knee flexion–extension axis. The attachment cuffs were adjusted to align the mechanical hinge with the estimated anatomical knee axis. Participants then performed repeated passive and low-speed active knee flexion–extension movements while the physiotherapist monitored alignment stability, cuff migration, observable relative motion between the limb and the device, and participant comfort. Minor adjustments were made when necessary to obtain smooth motion throughout the intended range of motion [52].

To address metabolic and comfort constraints, the mechanical design limits on-limb mass to below 3.5 kg through remote or proximal actuation, specifies peak torque capabilities of 0.4 Nm/kg for stance-phase extension and approximately 0.25 Nm/kg for swing-phase flexion. To satisfy the weight limit and reduce the mass moment of inertia, actuation is realized using a compact, high-torque DC motor rather than a Bowden-cable-driven SEA.

The actuation package comprises a brushless DC motor coupled to a gearhead with a reduction ratio of 80:1 to 120:1, providing a peak output torque of 30 N·m, a continuous torque of 15 N·m, and an operating speed range of 0–2 rad/s [53]. The selection of a peak output torque of 30 N·m is consistent with the range of assistive torques, 5 to 30 N.m reported for electrically actuated knee exoskeletons in the recent systematic review [58]. This value represents the maximum output capacity of the motor–gearhead assembly rather than the torque required continuously during rehabilitation. A rotary encoder with a resolution of 10,000 counts per revolution and an integrated torque sensor are incorporated to monitor joint angle and measure output torque, respectively; the combined motor-gearbox mass is limited to a maximum of 1.5 kg to preserve overall system portability and patient comfort. By prioritizing mechanical simplicity, light weight, and ease of use, the proposed design achieves a favorable trade-off between biomechanical compatibility and practical usability, rendering it suitable for both clinical and home-based deployment following initial physiotherapist supervision.

In addition to the extracted design features, the design objectives are outlined with consideration for compatibility with recommended by the American Academy of Orthopedic surgeons, along with adherence to ISO 13482 and IEC 60601 ethical and safety standards.

To translate the remaining design targets (summarized in Table 1) into a physical embodiment, anthropometric data drawn from the ANSUR II database and NASA STD-3001 standards were employed to establish link dimensions appropriate for a patient height range of 150–190 cm, yielding thigh and shank lengths of 40–45 cm and 35–40 cm, respectively, with link widths of 40–50 mm and a 4 mm wall thickness. The structural links and frames are fabricated from 7075 T6 aluminum alloy to achieve a lightweight yet high-stiffness construction. Titanium Grade 5 fasteners are specified for their superior strength and tissue compatibility. Medical-grade silicone contact pads provide skin-safe, shock-absorbing interfaces. Biological evaluation of these materials, would be conducted in accordance with ISO 10993-1:2025, including assessment of sensitization under Clause 6.5.3. The unilateral exoskeleton interfaces with a single lower limb via attachment points at the mid-thigh (proximal one-third) and the shank just below the tibial tuberosity (distal one-third), with anthropometric alignment achieved through adjustable semi-rigid cuff straps incorporating hook-and-loop fasteners, integrated padding, and mechanical guides that ensure the knee joint axis coincides with the user's anatomical knee center.

For sustained interface comfort, breathable textiles combined with a minimum of 10 mm EVA foam cushioning are specified.

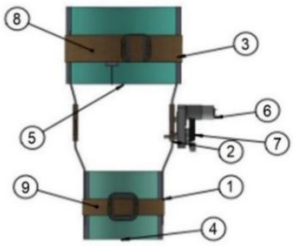


Fig. 1 The CAD model of the proposed robotic-assisted system, parts of the robot include, (1) shank's side support, (2) actuator support, (3) thigh's side support, (4) shank's brace, (5) thigh's brace, (6) DC motor and gearbox, (7) Arduino microcontroller, (8) force sensor, (9) straps.

Furthermore, their biocompatibility would be assessed in accordance with ISO 10993-1:2025, including evaluation of sensitization under Clause 6.5.3 and irritation under Clause 6.5.4.

2-5- Finite Element Analysis and Structural Validation

The proposed CAD model was imported into ANSYS 2024 R1 for finite element analysis. The simulations evaluated the exoskeleton's structural integrity, deformation, and stress distribution under clinically representative loading conditions. Boundary conditions include a fixed support at the proximal thigh connector, frictional contact at joint interfaces, and interaction forces transmitted through the thigh and shank cuffs. Because the FEM isolates the metallic exoskeleton structure, comprising Al 7075-T6 links, hinge joints, and cuff brackets, the applied loads are classified into human-side biological loads and exoskeleton-side loads and boundary conditions. The human-side loads comprise a 1200 N gravitational load, representing an assumed upper-bound design load for evaluating the biomechanical loading conditions, and a 150 N upward vertical foot-reaction force, selected as a representative engineering load for simulating partial weight-bearing during early postoperative rehabilitation following TKA. The selection of the partial weight-bearing scenario is informed by a prospective clinical study of 50 patients after TKA, in which patients were instructed to limit loading of the operated limb to 200 N [55]. These loads describe the intended human biomechanical loading scenario and are not directly measured in this research and not applied to the exoskeleton links in the present structural model. The exoskeleton-side boundary conditions include a fixed support at the proximal thigh connector bracket, constraining all translational and rotational degrees of freedom, and a 30 N·m rotational moment applied about the revolute knee hinge axis to represent the peak output torque of the motor–gearbox assembly. Additionally, distributed cuff-interface loads of 20 N normal to the inner contact surfaces and 60 N tangential to the limb interfaces are prescribed as representative engineering design loads to simulate radial compression and longitudinal retention at the thigh and shank cuffs, respectively. The selection of these loads was informed by studies highlighting the importance of characterizing human–exoskeleton interaction forces for contact safety and skin-injury risk assessment [56–57]. Accordingly, both values represent modeling inputs for evaluating the structural response of the exoskeleton under the specified loading conditions, rather than patient-specific measurements of human–exoskeleton contact forces. The exoskeleton's self-weight is incorporated as a gravitational body force of 9.81 m/s² acting throughout the solid model, corresponding to a total device mass of 3.5 kg and an approximate weight of 34.34 N.

Since the dynamic simulation inherently accounts for inertial effects, motion-reversal transients, and frictional contact nonlinearities, all of which produce stress and deformation responses that bound the corresponding static equivalents, the dynamic results conclusively supersede any independent static case.

Table 2 Material properties for the structural elements of robot

	AL 7075 T6	Titanium Grade 5	Pads (Medical-Grade Silicone)
Density (kg/m3)	2810	4430	1100
Young's Modulus (GPa)	71.7	113.8	300
Poisson's Ratio	0.33	0.34	0.49
Yield Strength (MPa)	503	880	
Ultimate Strength (MPa)	572	895	

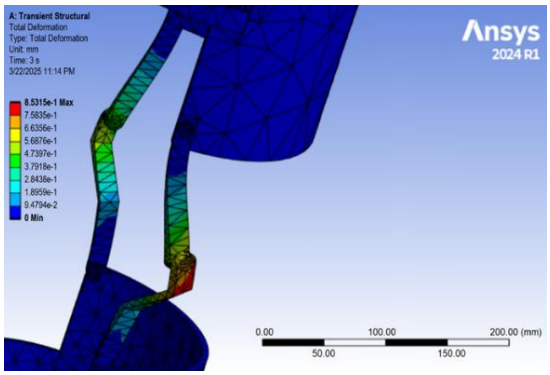


Fig. 2 Total deformation of the robotic-assisted system subjected to dynamic loading.

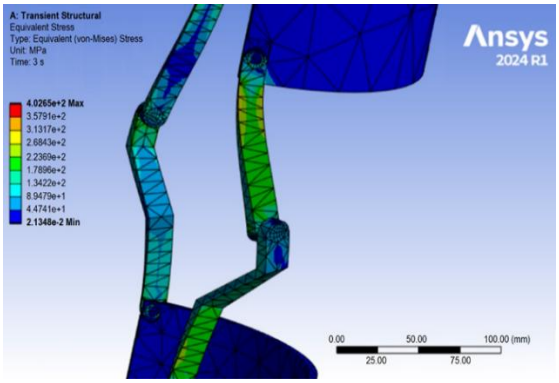


Fig. 3 The von-Mises stress contour plot of the robotic-assisted system subjected to dynamic loading.

Mechanical properties for the 7075-T6 aluminum alloy structural components, titanium Grade 5 fasteners, and medical-grade silicone pads were assigned according to the values summarized in Table 2.
The dynamic loading analysis yields a maximum deformation of 0.85 mm, as indicated in Fig. 2 and a peak von Mises stress of 172.8 MPa, as illustrated in Fig. 3 at the hinge and cuff interfaces during motion reversal. Both values remain well within permissible safety thresholds, confirming the design's structural robustness, compliance with IEC 60601 1 safety standards, and suitability for early phase post TKA rehabilitation.

2-6- Multi-Objective Optimization and Final Design

The FEM simulation results presented in Fig. 2 and 3 indicate that the proposed mechanical structure exhibits excessive rigidity. Optimization is essential for enhancing structural safety, patient comfort, weight reduction, while also improving cost-effectiveness and manufacturability of the exoskeleton for post-TKA rehabilitation. A dual-objective optimization was formulated to minimize both the peak interaction force between the exoskeleton and the user, and the stress amplitude in structural components, subject to a total device weight constraint not exceeding approximately 4% of the user's body weight, capped at 3.5 kg. This formulation ensures user comfort and structural safety, both critical for wearable rehabilitation devices.
Parametric modeling and response surface-based optimization were performed using the DesignXplorer module of ANSYS Workbench. Design variables were selected based on their significant influence on stress distribution, stiffness, and overall mass of the exoskeleton. The primary geometric design variables included the link length between the knee joint axis and the cuff attachment, link thickness, cross-sectional width, and the material was fixed as Al 7075-T6. The initial values and their bounds for link length, link thickness, and cross-sectional area, were set to 150 mm [120–200 mm], 4 mm [3.0–6.0 mm], and 160 mm² [50.0–200.0 mm²], respectively. Furthermore, The normal and tangential human–exoskeleton interface forces were defined separately as prescribed design-loading parameters, with nominal values and their bounds of 20 N [10–30 N] and 60 N [30–90 N], respectively, to account for variability in interface loading.
The optimization problem was defined as a multi-objective minimization:

$$\text{Minimize } f_1 = \omega_1 \frac{F_{\text{interface}}(x)}{F_m} + \omega_2 \frac{\sigma_{\text{amplitude}}(x)}{\sigma_m} \quad (1)$$

$$\omega_1 + \omega_2 = 1 \quad (2)$$

where, $F_{\text{interface}}$, $\sigma_{\text{amplitude}}$, F_m, σ_m, ω_1, ω_2 and x represent the interaction force between the exoskeleton and the user, which was obtained through FEM analysis and dynamic simulation, stress amplitude in the exoskeleton frame, reference interaction force between the exoskeleton and the user, reference stress amplitude in the exoskeleton frame, weighting factors to balance the two objectives, and design variables, respectively. The amplitude of the reference interaction force, and reference stress are considered as 63.25 N, and 172.8 MPa, respectively. The optimization was subjected to the following mass constraint:

$$\text{Weight}(x) \leq 0.04\, m_{\text{user}}.\, g \quad (3)$$

with m_{user} = 80 kg, represent user mass, and g = 9.81 m/s². The operating condition assumed a constant angular velocity of 1 rad/s, and boundary conditions included the actuator assistive torque, gravitational load, vertical reaction force, and interaction forces.

3- Results

The FEM-based optimization was applied to the initial conceptual design, yielding final link thickness and cross-sectional area of 3.6 mm and 165 mm², respectively, with a minimum system mass of 2.8 kg. As illustrated in Fig. 4, the total deformation under dynamic loading was reduced to 0.62 mm, a 27% reduction over the pre-optimization value of 0.85 mm, well within the ISO 13482 limit of 2 mm and indicative of enhanced structural stiffness. The von Mises stress contour plot in Fig. 5 shows a peak stress of 143.9 MPa at the hinge and attachment interfaces, representing a 13.2% reduction from the pre-optimization dynamic peak of 172.8 MPa, while remaining substantially below the yield strength with no plastic deformation risk. The optimized design achieves a more uniform load distribution and improved stress gradients through geometric refinements, increasing the fatigue safety factor from 1.39 to 1.67 across critical regions. Additionally, the optimization resulted in a 30% reduction in cuff interaction force, enhancing patient comfort and minimizing skin irritation risks, thereby rendering the system suitable for both clinical and home-based rehabilitation settings.
Following the optimization process, further static structural analysis was performed to independently assess the structural integrity of the optimized knee exoskeleton under the prescribed loading conditions. As shown in Fig. 6, the equivalent von Mises stress distribution indicates a maximum stress of 135.8 MPa, concentrated around the hinge region of the multi-joint levers, where localized stress concentrations are expected due to load transfer through the joints.

This value is substantially below the nominal yield strength of 7075-T6 aluminum alloy, indicating that the optimized structure remains below the material's yield limit under the analyzed static loading conditions.

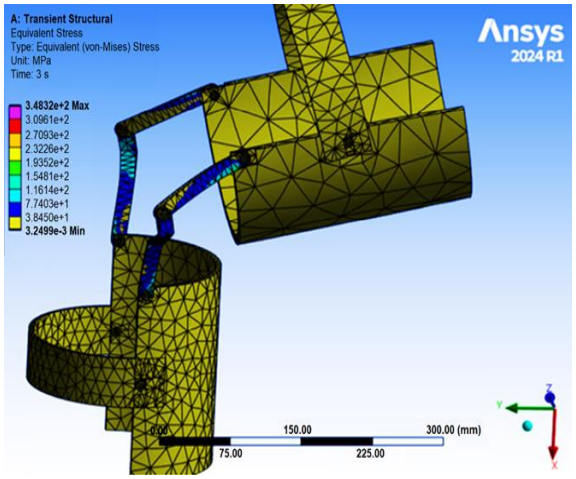


Fig. 4 Total deformation of the robotic-assisted system after optimization subjected to dynamic loading.

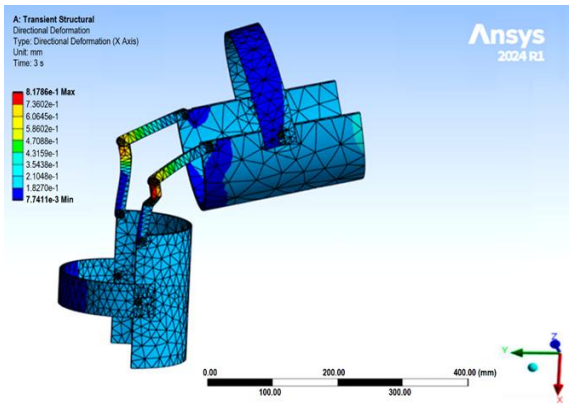


Fig. 5 The von-Mises stress contour plot of the robotic-assisted system after optimization subjected to dynamic loading.

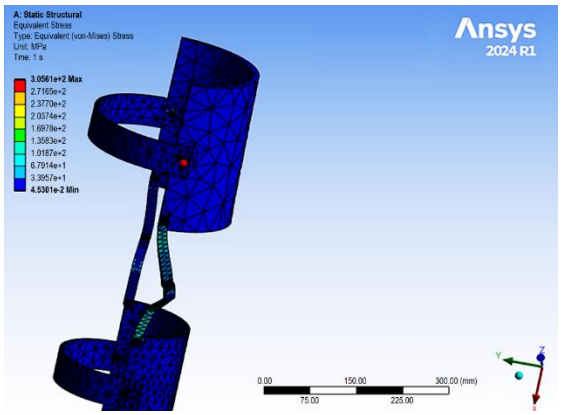
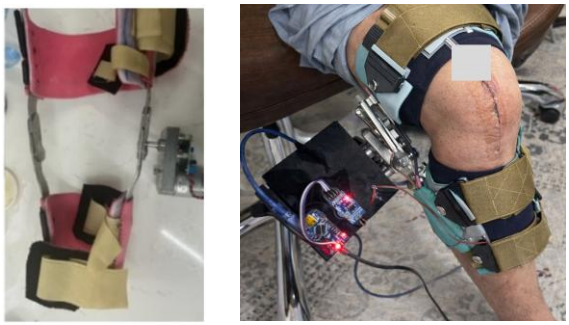


Fig. 6 The von-Mises stress contour plot of the robotic-assisted system after optimization subjected to static loading.

4- Experimental Prototyping

To validate the proposed optimized design, an experimental prototype of the robotic assisted system was fabricated. The prototype is presented in Fig. 7(a), with the setup used on a patient's limb in Fig. 7(b). Links and frames of the robot, were manufactured from 7075 T6 aluminum alloy, selected for its superior stiffness to weight ratio, and high fatigue resistance. Fasteners were fabricated from Grade 5 titanium, ensuring high strength and biocompatibility. To ensure user comfort and mitigate the risk of pressure-related irritation, the thigh and shank cuffs incorporate breathable textile layers with over 10 mm of EVA foam padding .

Actuation is provided by a brushless DC motor paired with a precision planetary gearbox, delivering high torque output with low noise and compatibility with standard 24 V DC power supplies. The bidirectional mechanism consumes 70 mA under no load conditions and up to 350 mA at full load, providing a reliable actuation profile for rehabilitation scenarios. The control system is built using an Arduino based platform centered on the ATmega328P microcontroller. This system featuring 14 digital I/O pins (PWM capable), 6 analog input channels, a 16 MHz crystal oscillator, USB and power inputs, and in circuit serial programming capability. Real time execution of predefined motion trajectories in control algorithms developed in C/C++, are compiled and uploaded via USB. The control architecture follows a modular flowchart structure incorporating key parameters, angular velocity and acceleration, joint torque, and operates within a continuous feedback loop that updates variables based on user defined targets.



(a) (b)

Fig. 7 (a) prototype of the exoskeleton, (b) the setup used on a patient's limb

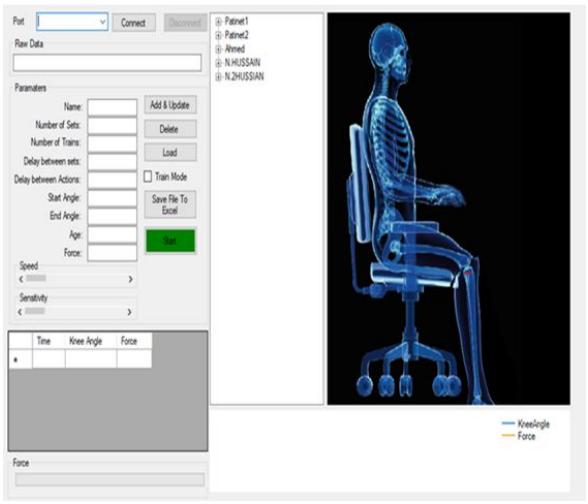


Fig. 8 The GUI was created using Visual Studio software for control of the rehabilitation exoskeletal robot.

To ensure patient safety, mechanical hard stops are integrated into the structure, with maximum angular velocity, acceleration, and torque specified as safety thresholds.

A user-friendly graphical interface (GUI) was developed using Microsoft Visual Studio to enable physiotherapists to configure and customize main rehabilitation parameters. The most important parameters can be set include motor speed, joint angular limits, repetition counts, rest durations, and torque thresholds. The modular interface design indicated in Fig. 8 facilitates the integration of different operating and control modes and allows for future monitoring of therapy progression.

5- Biomechanical Compatibility, Safety, and Outcome Evaluation Procedures

The design of knee exoskeletons for post-TKA rehabilitation must address four fundamental biomechanical compatibility challenges, each demanding targeted engineering solutions to ensure safe and effective device operation. First, the polycentric ICR trajectory of the anatomical knee is inherently mismatched by rigid single-axis hinges, which impose a fixed pivot and generate parasitic shear forces that directly challenge tibial and femoral implant fixation interfaces [37–38]. To mitigate this kinematic incompatibility, a clinical alignment procedure should be implemented. The exoskeleton was adjusted by an experienced physiotherapist following established clinical principles for CPM devices. The lateral femoral epicondyle was palpated to identify the anatomical reference for the knee flexion–extension axis. The thigh and shank segments and attachment cuffs were then adjusted to align visually with the participant's anatomical knee axis. Participants performed repeated passive and low-speed active flexion–extension movements. The physiotherapist monitored alignment stability, cuff migration, relative limb–device motion, and comfort. Adjustments were made until smooth, unrestricted movement was achieved throughout the intended ROM.

Second, viscoelastic deformation of skin, adipose, and muscle tissues at the physical human-exoskeleton interface absorbs actuation energy, introducing mechanical backlash, torque transmission delays, and axial cuff migration during cyclic motion, which reduces torque-tracking bandwidth and distorts encoder-based joint angle measurements [41, 47]. This is addressed through a multi-faceted approach employing rigid, anthropometrically contoured carbon-fiber/thermoplastic cuffs lined with high-friction, non-slip silicone elastomer padding to establish a firm interface with minimal slack.

Third, transmitting assistive moments requires substantial normal forces at the cuffs; however, excessive torque magnitudes or rapid torque application rates create localized pressure concentrations that compromise user comfort and force controller gains downward to avoid pain or soft-tissue bruising [47]. In post-surgical patients, such pressures near incisions can compromise healing tissue. To counteract this, wide, curved load-distributing cuffs are positioned proximally on the thigh and distally on the lower shank to maximize contact area and maintain interface forces at reduced levels (demonstrated at 44.3 N), avoiding wound edge tension. Peak allowable flexion/extension assistance magnitudes are bounded at 0.25–0.5 N·m/kg, and spline nodes are configured to limit torque rate of increase, preventing impulse spikes and discomfort. Dedicated cut-outs and soft neoprene relief zones are incorporated around the anterior midline and lateral arthrotomy sites to prevent direct mechanical contact or shear near the healing scar.

Finally, distal limb mass significantly increases metabolic cost [39], necessitating proximally mounted actuation to minimize inertial penalties and preserve therapeutic unloading effects [41, 47]. Accordingly, high-power DC motor paired with a precision planetary gearbox, minimizing on-limb mass. Structural links are optimized and constructed using high-strength Al 7075-T6 aluminum, and the exoskeleton's center of mass is repositioned proximally toward the knee axis to reduce rotational inertia and gravitational loading on the quadriceps.

Prior to human trials, pre-clinical benchtop verification is essential to ensure that all physical and control fail-safes are fully operational, guaranteeing safe device operation. Mechanical end-stops are configured at 0° to prevent hyperextension and capped at 90° (acute) and 120° (subacute). Emergency stops and software torque thresholds are validated to trip within <10 ms when resistance exceeds 0.6–0.8 N·m/kg [41, 53]. The clinical alignment procedure described above was consistently applied during fitting.

The procedure for the fabricated prototype, which must be conducted prior to clinical trials, is structured in two phases, with outcome evaluation spanning four weeks. Detailed procedures are described in the following sections.

Phase I validation will involve 3–5 healthy volunteers to evaluate kinematic compatibility, interface pressure, control fidelity, and muscle activation patterns.

Kinematic trajectory tracking error is maintained below 2° using 3D motion capture, with no joint migration or cuff slippage. Thin-film pressure sensors confirm peak skin interface pressure remains below 32 mmHg to prevent necrosis. Device operation avoids rapid or unnatural joint extensions that could cause discomfort [47]. Real-time torque/encoder logs validate smooth transitions between CPM, stance stiffness, and swing damping modes. Surface EMG of vastus lateralis, rectus femoris, and hamstrings verifies that AAN control reduces muscle effort without inducing antagonist co-contraction [47], consistent with human-in-the-loop paradigms [55].

Phase II constitutes a clinical pilot on post-TKA patients (post-op days 3–14 or subacute weeks 2–6). Objective orthopedic metrics include active vs. passive ROM (target: 0° extension deficit; progressive flexion ≥90°–110°), quantified via robotic encoders and independent goniometry. Quadriceps reactivation is assessed through reduction of active extension lag during seated leg-raise exercises, while ambulatory testing measures vertical ground reaction forces (vGRF) to confirm limb symmetry and stance stability [59]. Subjective outcomes include VAS pain scores (session ΔVAS $\leq$2), wound inspection for erythema or dehiscence, standardized clinical scores (KOOS, WOMAC), and functional mobility tests [56], integrated with quantitative robotic data [60]. User acceptance is quantified via the system usability scale, assessing safety, comfort, and don/doff ease.

A 4-week evaluation protocol progresses through three phases, mirroring the multi-stage rehabilitation trajectory [61]: Week 1 employs CPM mode (seated/supine, 0°–90°) to prevent arthrofibrosis; Weeks 2–3 transition to AAN mode for quadriceps voluntary torque recovery and extension lag elimination; Week 4 introduces stance stabilization and overground ambulation using state-based impedance control to verify stance support and swing clearance during level walking.

6- Discussions

The FEA-guided optimization improved the structural design of the one-DOF knee exoskeleton, balancing structural safety, and ergonomic considerations, for post-TKA rehabilitation.

The structural performance of the optimized exoskeleton was evaluated using static and dynamic analyses. Both analyses used the same optimized geometry, material properties, support conditions, and corresponding load components. They differed only in the analysis formulation and treatment of time-dependent effects. The maximum von Mises stresses were compared to assess the influence of dynamic effects on the structural response and stress concentrations at critical locations. Under dynamic loading conditions, the optimized configuration, characterized by a total mass of 2.8 kg, a link thickness of 3.6 mm, and a cross-sectional area of 165 mm², exhibited a peak von Mises stress of 143.9 MPa. This represented a reduction from the pre-optimization value of 172.8 MPa; however, the reduction is approximately 16.7%, rather than 13.2%. The calculated peak stress

was also below the reported endurance limit of 159 MPa for 7075-T6 aluminum alloy. Furthermore, the fatigue safety factor increased from 1.39 to 1.67, corresponding to an improvement of approximately 20.1%. The fatigue assessment, based on the Goodman mean-stress correction, provided an estimate of fatigue performance under the specified loading assumptions [41]. These results suggest improved structural performance following optimization. Overall, the analyses provide complementary evidence of the optimized design's structural performance under the modeled conditions, but do not independently establish clinical performance or long-term durability under actual rehabilitation use.

Maximum structural deformation under dynamic loading was reduced by 27%, from 0.85 mm to 0.62 mm (Fig. 4), maintaining the internal design limit <2 mm, while preserving kinematic accuracy across the full flexion/extension range [41]. Concurrently, cuff-limb interaction forces decreased by 30%, from 63.3 N to 44.3 N, substantially reducing soft-tissue injury risk [56–57, 62]. The optimized design reduced the exoskeleton mass to 2.8 kg, potentially reducing device-induced limb mass and rotational inertia. Although previous studies have linked lower-limb mass to walking energetics and biomechanics [39], metabolic cost was not measured and any reduction remains to be experimentally verified. A total system mass of 2.8 kg is within the viable range for single-joint knee orthoses [41, 47].

The optimization also repositioned the exoskeleton's CoM closer to the knee joint axis, from 112 mm distal and 28 mm anterior to 96 mm distal and 19 mm anterior, minimizing the distal gravitational moment and rotational inertia about the knee. This reduction in passive torque decreases quadriceps effort for joint stabilization, a critical benefit for post-TKA patients, while enhancing dynamic balance and user confidence during early-stage rehabilitation [47].

Global sensitivity analysis using Sobol indices identified link thickness as the dominant stress control variable (Sobol index: 0.58), where a 10% increase reduced peak stress by 18.3% at a 7.2% mass penalty, while cross-sectional area governed deformation control (26.4% reduction for a 12% mass cost). Material properties exhibited negligible influence (Sobol indices: 0.01 for yield strength, 0.09 for density), validating the retention of Al 7075-T6. The significant coupling between thickness and area (14% stress variance) confirmed the necessity of simultaneous optimization, as isolated adjustments would have failed to achieve the target performance [41]. This geometric sensitivity hierarchy, thickness for stress mitigation and width for stiffness control, establishes a generalizable heuristic for rehabilitation exoskeletons.

It should be noted that, while the developed 2.8 kg prototype establishes a rigorous mechanical, structural, and mechatronic foundation for post-TKA rehabilitation, limitations of the present study are that experimental evaluations were restricted to bench-level characterization. Structural performance of the proposed exoskeleton has not yet been experimentally validated through quantitative comparison of FEM predictions with physical test results. Furthermore, assessing the clinical efficacy and user-adaptation of the device on actual post-TKA patients requires formal institutional ethical approval and clinical site permissions. Consequently, comprehensive clinical trials involving human subjects are currently being organized under approved medical ethical frameworks as a primary direction for future work, building directly upon the foundational design and kinematic safety validated in this study.

7- Conclusions

This study presents a complete literature-to-prototype engineering methodology for the development of a dedicated 1-DOF robotic knee exoskeleton intended for post-TKA rehabilitation. Systematic feature extraction from the lower-extremity exoskeleton literature established that isolated knee rehabilitation does not require bulky multi-joint hardware; rather, it depends on targeted sagittal-plane torque assistance, anatomical axis compatibility, minimal distal inertia, and adaptive state-based impedance control. FEA-driven structural optimization proved essential in resolving the inherent trade-offs between structural rigidity, lightweight construction, and soft-tissue safety. By coupling geometric dimensions with the mechanical properties of Al 7075-T6, the optimized linkage achieved fatigue resistance exceeding infinite operational life cycle while strictly constraining peak deflection to 0.62 mm and reducing cuff interaction forces to 44.3 N. Furthermore, proximal relocation of the exoskeleton's CoM minimizes distal inertial penalties and reduces passive loading on the healing quadriceps during early rehabilitation. The resulting 2.8 kg prototype constitutes an effective, lightweight, and safe mechatronic platform that can support subsequent clinical evaluation of progressive post-TKA knee mobilization.

Artificial Intelligence Statement: During the preparation of this work, the authors utilized DeepSeek solely for language refinement, grammar correction, and stylistic improvements to enhance readability and clarity. Following the use of these tools, the authors thoroughly reviewed and edited the content as necessary and take full responsibility for the final published manuscript. No generative AI tools were employed for data analysis, experimental design, result interpretation, or the generation of scientific conclusions.

Acknowledgements: The authors would like to express their sincere gratitude to the medical and rehabilitation teams at Al-Zahra Clinic, Marjan Medical Hospital, and the Babylon Rehabilitation Center for their invaluable support during the pre-clinical evaluation phase of this study. Special appreciation is extended to the engineering and technical staff of the Robotics Laboratory at Alfurat Al-Awsat Technical University for their dedicated assistance in prototyping, instrumentation, and experimental testing.

Funding: The authors declare that this research was conducted without any financial support from funding agencies in the public, commercial, or not-for-profit sectors.

CRediT Authorship Contribution: Conceptualization, Methodology, Software, Validation, Formal Analysis, Investigation, Resources, Data Curation, Visualization, Writing – Original Draft, and Funding Acquisition: Raed Abdulameer Mahmood Alalvani;
Writing – Review & Editing, Supervision, and Project Administration: Ali Selk Ghafari.
All authors have read and agreed to the published version of the manuscript.

Conflict of Interest: The authors declare that they have no competing financial or personal interests that could have influenced the research presented in this paper. The findings reported are part of the Ph.D. dissertation of the first author, and the authors confirm that no conflicts of interest are associated with this study.

References

[1] C. Vandepitte, L. Van Pachtenbeke, I. Van Herreweghe, R. K. Gupta, and N. M. Elkassabany, "Same day joint replacement surgery: Patient selection and perioperative management," *Anesthesiol. Clin.*, vol. 40, no. 3, pp. 537–545, 2022. doi: 10.1016/j.anclin.2022.04.003.

[2] R. B. Salter, H. W. Hamilton, J. H. Wedge, M. Tile, I. P. Torode, S. W. O'Driscoll, J. J. Murnaghan, and J. H. Saringer, "Clinical application of basic research on continuous passive motion for disorders and injuries of synovial joints: A preliminary report of a feasibility study," *J. Orthop. Res.*, vol. 1, no. 3, pp. 325–342, 1984. doi: 10.1002/jor.1100010313.

[3] L. A. Bennett, S. C. Brearley, J. A. L. Hart, and M. J. Bailey, "A comparison of 2 continuous passive motion protocols after total knee arthroplasty: A controlled and randomized study," *J. Arthroplasty*, vol. 20, no. 2, pp. 225–233, Feb. 2005. doi: 10.1016/j.arth.2004.08.009.

[4] R. N. Maniar, J. V. Baviskar, T. Singhi, and S. S. Rathi, “To use or not to use continuous passive motion post–total knee arthroplasty,” *J. Arthroplasty*, vol. 27, no. 2, pp. 193–200, Feb. 2012. doi: 10.1016/j.arth.2011.04.009.

[5] A. B. Imhoff, K. Beitzel, K. Stamer, E. Klein, and G. Mazzocca, Eds., *Rehabilitation in Orthopedic Surgery*. Berlin, Heidelberg, Germany: Springer Berlin Heidelberg, 2016. doi: 10.1007/978-3-662-49149-2.

[6] Y. Sankai, “HAL: Hybrid assistive limb based on cybernics,” in *Robotics Research*, M. Kaneko and Y. Nakamura, Eds. Berlin, Heidelberg, Germany: Springer Berlin Heidelberg, 2010, pp. 25–34. doi: 10.1007/978-3-642-14743-2_3.

[7] EksoHealth | Ekso Bionics. [Online]. Available: https://eksobionics.com/eksohealth/products/

[8] S. A. Kolakowsky-Hayner, J. Crew, S. Moran, and A. Shah, “Safety and feasibility of using the EksoTM bionic exoskeleton to aid ambulation after spinal cord injury,” *J. Spine*, vol. 4, no. 3, 2013. doi: 10.1080/10790268.2019.1671076.

[9] R. Little and R. A. Irving, “Self contained powered exoskeleton walker for a disabled user,” U.S. Patent 2011/0066088 A1, Mar. 17, 2011.

[10] M. A. Beirne, K. Nedley, S. Wallis, and G. E. Francisco, “A treatment proposal with lower extremity robotic devices: Performance of postural analysis and determination of exercises using the REX robot,” TIRR Memorial Hermann – Rehabilitation & Research.

[11] R. Bogue, “Exoskeletons and robotic prosthetics: A review of recent developments,” *Ind. Robot*, vol. 36, no. 5, pp. 421–427, Aug. 2009. doi: 10.1108/01439910910980141.

[12] K. Raab, K. Krakow, F. Tripp, and M. Jung, “Effects of training with the ReWalk exoskeleton on quality of life in incomplete spinal cord injury: A single case study,” *Spinal Cord Ser. Cases*, vol. 2, p. 15025, 2016. doi: 10.1038/scsandc.2015.25.

[13] Indego – Powering People Forward | Parker Indego. [Online]. Available: http://www.indego.com/indego/en/home.

[14] PHOENIX Medical Exoskeleton | suitX. [Online]. Available: https://www.suitx.com/phoenix-medical-exoskeleton

[15] B. Celebi, M. Yalcin, and V. Patoglu, “AssistOn-Knee: A self-aligning knee exoskeleton,” in *2013 IEEE/RSJ Int. Conf. Intell. Robots Syst. (IROS)*, Tokyo, Japan, Nov. 2013, pp. 996–1002. doi: 10.1109/IROS.2013.6696472.

[16] A. Taherifar, G. Vossoughi, and A. Selk Ghafari, "Identification and torque control of series elastic actuator of lower limb extremity exoskeleton," *Modares Mech. Eng.*, vol. 17, no. 8, pp. 1–8, 2017. Dor: 20.1001.1.10275940.1396.17.8.38.2

[17] V. A. D. Cai, P. Bidaud, T. T. Le, A. Ibanez, and X. T. Phan, “In search of transparency for lower limb exoskeleton devices with a new mechanical design and a robust gait phases detection method,” in *2015 IEEE Int. Conf. Robot. Biomim. (ROBIO)*, Zhuhai, China, Dec. 2015, pp. 1151–1156. doi: 10.1109/ROBIO.2015.7418927.

[18] M. Wehner et al., “A lightweight soft exosuit for gait assistance,” in *2013 IEEE Int. Conf. Robot. Autom. (ICRA)*, Karlsruhe, Germany, May 2013, pp. 3362–3369. doi: 10.1109/ICRA.2013.6631046.

[19] S. Hosseinpour Malakouti and S. Ozgoli, "Design, control, and experimental evaluation of a lightweight active knee–ankle–foot orthosis with adjustable knee motion for mobility assistance after spinal cord injury," *Modares Mech. Eng.*, vol. 26, no. 4, pp. 261–269, 2026. doi: 10.48311/mme.2026.118299.82908.

[20] R. Wilmart, E. Garone, and B. Innocenti, “The use of robotics devices in knee rehabilitation: A critical review,” *Muscle Ligaments Tendons J.*, vol. 9, no. 1, pp. 21–48, 2019. doi: 10.32098/mltj.01.2019.07.

[21] S. Hesse, A. Waldner, and C. Tomelleri, “Innovative gait robot for the repetitive practice of floor walking and stair climbing up and down in stroke patients,” *J. Neuroeng. Rehabil.*, vol. 7, p. 30, Jun. 2010. doi: 10.1186/1743-0003-7-30.

[22] G. Colombo, M. Joerg, R. Schreier, and V. Dietz, "Treadmill training of paraplegic patients using a robotic orthosis," *J. Rehabil. Res. Dev.*, vol. 37, no. 6, pp. 693–700, Nov. 2000. PMID: 11321005.

[23] S. Freivogel, J. Mehrholz, T. Husak-Sotomayor, and D. Schmalohr, "Gait training with the newly developed 'LokoHelp'-system is feasible for non-ambulatory patients after stroke, spinal cord and brain injury. A feasibility study," *Brain Injury*, vol. 22, no. 7–8, pp. 625–632, Jul. 2008. doi: 10.1080/02699050801941771.

[24] S. K. Banala, S. K. Agrawal, and J. P. Scholz, "Active leg exoskeleton (ALEX) for gait rehabilitation of motor-impaired patients," in *Proc. 10th IEEE Int. Conf. Rehabil. Robot. (ICORR)*, Noordwijk, The Netherlands, Jun. 2007, pp. 401–407. doi: 10.1109/ICORR.2007.4428456.

[25] J. F. Veneman, R. Kruidhof, E. E. G. Hekman, R. Ekkelenkamp, E. H. F. Van Asseldonk, and H. Van Der Kooij, "Design and evaluation of the LOPES exoskeleton robot for interactive gait rehabilitation," *IEEE Trans. Neural Syst. Rehabil. Eng.*, vol. 15, no. 3, pp. 379–386, Sep. 2007. doi: 10.1109/TNSRE.2007.903919.

[26] S. Hesse, D. Uhlenbrock, C. Werner, and A. Bardeleben, "A mechanized gait trainer for restoring gait in nonambulatory subjects," *Arch. Phys. Med. Rehabil.*, vol. 81, no. 9, pp. 1158–1161, Sep. 2000. doi: 10.1053/apmr.2000.6280.

[27] H. Schmidt, S. Hesse, R. Bernhardt, and J. Krüger, "HapticWalker—a novel haptic foot device," *ACM Trans. Appl. Percept.*, vol. 2, no. 2, pp. 166–180, Apr. 2005. doi: 10.1145/1060581.1060589.

[28] H. Yano, S. Tamefusa, N. Tanaka, H. Saitou and H. Iwata, "Gait rehabilitation system for stair climbing and descending," *2010 IEEE Haptics Symposium*, Waltham, MA, USA, 2010, pp. 393-400, doi: 10.1109/HAPTIC.2010.5444627.

[29] M. Peshkin, D. A. Brown, J. J. Santos-Munne, A. Makhlin, E. Lewis, J. E. Colgate, J. Patton, and D. Schwandt, "KineAssist: A robotic overground gait and balance training device," in *Proc. 9th IEEE Int. Conf. Rehabil. Robot. (ICORR)*, Chicago, IL, USA, Jun. 2005, pp. 241–246. doi: 10.1109/ICORR.2005.1501094.

[30] M. Bouri, Y. Stauffer, C. Schmitt, Y. Allemand, S. Gnemmi, R. Clavel, P. Metrailler, and R. Brodard, "The WalkTrainer: A robotic system for walking rehabilitation," in *Proc. IEEE Int. Conf. Robot. Biomim. (ROBIO)*, Kunming, China, Dec. 2006, pp. 1616–1621. doi: 10.1109/ROBIO.2006.340186.

[31] H. Kawamoto and Y. Sankai, "Power assist system HAL-3 for gait disorder person," in *Computers Helping People with Special Needs*, K. Miesenberger, J. Klaus, and W. Zagler, Eds., (Lecture Notes in Computer Science, vol. 2398), Berlin, Heidelberg: Springer, 2002, pp. 196–203. doi: 10.1007/3-540-45491-8_43.

[32] H. Kawamoto, T. Hayashi, T. Sakurai, K. Eguchi, and Y. Sankai, "Development of single leg version of HAL for hemiplegia," in *Proc. 31st Annu. Int. Conf. IEEE Eng. Med. Biol. Soc. (EMBC)*, Minneapolis, MN, USA, Sep. 2009, pp. 5038–5043. doi: 10.1109/IEMBS.2009.5333698.

[33] H. Schmidt, "HapticWalker—A novel haptic device for walking simulation," in *Proc. EuroHaptics Conf.*, Munich, Germany, Jun. 2004, pp. 60–67.

[34] M. Girone, G. Burdea, M. Bouzit, V. Popescu, and J. E. Deutsch, "Stewart platform-based system for ankle telerehabilitation," *Auton. Robots*, vol. 10, no. 2, pp. 203–212, Mar. 2001. doi: 10.1023/A:1008938121020.

[35] J. Nikitczuk, B. Weinberg, P. K. Canavan, and C. Mavroidis, "Active knee rehabilitation orthotic device with variable damping characteristics implemented via an electrorheological fluid," *IEEE/ASME Trans. Mechatronics*, vol. 15, no. 6, pp. 952–960, Dec. 2010. doi: 10.1109/TMECH.2009.2036170.

[36] E. Reznick, K. R. Embry, R. Neuman, E. Bolívar-Nieto, N. P. Fey, and R. D. Gregg, "Lower-limb kinematics and kinetics during continuously varying human locomotion," *Sci. Data*, vol. 8, p. 282, 2021. doi: 10.1038/s41597-021-01057-9.

[37] A. Asker, M. Omar, J. Zhang, K. Wang, R. Li, and S. Xie, "Optimum design of polycentric knee hinges based on analysis of knee-exoskeleton closed kinematic chain," *Proc. Inst. Mech. Eng. C*, vol. 239, no. 11, pp. 4085–4098, 2025. doi: 10.1177/09544062251313926.

[38] S. Patrick, N. Anil Kumar, and P. Hur, "Evaluating knee mechanisms for assistive devices," *Front. Neurorobot.*, vol. 16, Art. ID 790070, May 2022. doi: 10.3389/fnbot.2022.790070.

[39] R. C. Browning, J. R. Modica, R. Kram, and A. Goswami, "The effects of adding mass to the legs on the energetics and biomechanics of walking," *Med. Sci. Sports Exerc.*, vol. 39, no. 3, pp. 515–525, Mar. 2007. doi: 10.1249/mss.0b013e31802b3562.

[40] G. M. Bryan, P. W. Franks, S. C. Klein, R. J. Peuchen, and S. H. Collins, "A hip-knee-ankle exoskeleton emulator for studying gait assistance," *Int. J. Robot. Res.*, vol. 40, pp. 722–746, 2020. doi: 10.1177/0278364920961452.

[41] M. S. Ashrafi, M. Nazari, N. Sepehry, M. Mahdizadeh Rokhi, P. Samimi, and M. Attarchi, "Design and implementation of a fuzzy output feedback assistive controller for a series-elastic-actuator-driven knee exoskeleton," *Modares Mech. Eng.*, vol. 22, no. 8, pp. 541–553, 2022. doi: 10.52547/mme.22.8.541.

[42] T. Kikuchi, K. Oda, and J. Furusho, "Leg-robot for demonstration of spastic movements of brain-injured patients with compact magnetorheological fluid clutch," *Adv. Robot.*, vol. 24, no. 16, pp. 671–686, 2010. doi: 10.1163/016918610X496621.

[43] J. E. Pratt, B. T. Krupp, C. J. Morse, and S. H. Collins, "The RoboKnee: An exoskeleton for enhancing strength and endurance during walking," in *Proc. IEEE Int. Conf. Robot. Autom. (ICRA)*, New Orleans, LA, USA, May 2004, vol. 3, pp. 2430–2435. doi: 10.1109/ROBOT.2004.1307561.

[44] M. K. Shepherd and E. J. Rouse, "Design and validation of a torque-controllable knee exoskeleton for sit-to-stand assistance," *IEEE/ASME Trans. Mechatronics*, vol. 22, no. 4, pp. 1695–1704, Aug. 2017. doi: 10.1109/TMECH.2017.2704588.

[45] S. Mazzoleni, A. Focacci, M. Franceschini, A. Waldner, C. Spagnuolo, E. Battini, and D. Bonaiuti, "Robot-assisted end-effector-based gait training in chronic stroke patients: A multicentric uncontrolled observational retrospective clinical study," *NeuroRehabilitation*, vol. 40, no. 4, pp. 483–492, 2017. doi: 10.3233/NRE-161435.

[46] J. L. Emken, S. J. Harkema, J. A. Beres-Jones, C. K. Ferreira, and D. J. Reinkensmeyer, "Feasibility of manual teach-and-replay and continuous impedance shaping for robotic locomotor training following spinal cord injury," *IEEE Trans. Biomed. Eng.*, vol. 55, no. 1, pp. 322–334, Jan. 2008. doi: 10.1109/TBME.2007.910683.

[47] P. W. Franks, G. M. Bryan, R. M. Martin, R. Reyes, A. C. Lakmazaheri, and S. H. Collins, "Comparing optimized exoskeleton assistance of the hip, knee, and ankle in single and multi-joint configurations," *Wearable Technol.*, vol. 2, p. e16, 2021. doi: 10.1017/wtc.2021.14.

[48] M. B. Näf, K. Junius, M. Rossini, C. Rodriguez-Guerrero, B. Vanderborght, and D. Lefeber, "Misalignment compensation for full human-exoskeleton kinematic compatibility: State of the art and evaluation," *ASME Appl. Mech. Rev.*, vol. 70, no. 5, Art. no. 050802, Sep. 2018, doi: 10.1115/1.4042523.

[49] V. A. D. Cai, P. Bidaud, V. Hayward, F. Gosselin and E. Desailly, "Self-adjusting, isostatic exoskeleton for the human knee joint," *2011 Annual International Conference of the IEEE Engineering in Medicine and Biology Society*, Boston, MA, USA, 2011, pp. 612-618, doi: 10.1109/IEMBS.2011.6090136.

[50] Y. Niu, Z. Song, and J. Dai, "Kinematic analysis and optimization of a planar parallel compliant mechanism for self-alignment knee exoskeleton," *Mechanical Sciences*, vol. 9, no. 2, pp. 405–416, 2018. doi: 10.5194/ms-9-405-2018.

[51] A. Schiele and F. C. T. van der Helm, "Influence of attachment pressure and kinematic configuration on pHRI with wearable robots," *Applied Bionics and Biomechanics*, vol. 6, no. 2, pp. 157–173, 2009, doi: 10.1080/11762320902879961.

[52] C. C. Norkin and D. J. White, *Measurement of Joint Motion: A Guide to Goniometry*, 5th ed. Philadelphia, PA: F. A. Davis Company, 2017.

[53] A. Nasr, K. Inkol, and J. McPhee, "Safety in wearable robotic exoskeletons: Design, control, and testing guidelines," *J. Mech. Robot.*, vol. 17, no. 5, pp. 1–13, 2025. doi: 10.1115/1.4066900.

[54] D. Karibzhanova, A. Niyetkaliyev, A. R. Khawaja, A. Zhaisanbek, Zeeshan, A. Utepbergen, P. K. Jamwal, K. Ozhikenov, A. Ozhikenova, Z. Alimbayeva, Z. Bigaliyeva, L. Bazarbay, and S. Didar, "State-of-the-art knee exoskeleton for gait assistance and rehabilitation: Systematic review," *JMIR Rehabil. Assist. Technol.*, vol. 13, Art. no. e94916, 2026, doi: 10.2196/94916.

[55] P. M. Anderson, T. Heinz, E. Scholmann, A. Eidmann, J. Arnholdt, M. Rudert, B. M. Holzapfel, and I. Stratos, "Efficacy of post-operative partial weight-bearing after total knee arthroplasty - a prospective observational trial," Int. Orthop., vol. 47, no. 9, pp. 2189–2195, Sep. 2023, doi: 10.1007/s00264-023-05783-0.

[56] X. Wan, Y. Liu, Y. Akiyama and Y. Yamada, "Monitoring Contact Behavior During Assisted Walking with a Lower Limb Exoskeleton," in IEEE Transactions on Neural Systems and Rehabilitation Engineering, vol. 28, no. 4, pp. 869-877, April 2020, doi: 10.1109/TNSRE.2020.2979986.

[57] Y. Akiyama, Y. Yamada, and S. Okamoto, "Interaction forces beneath cuffs of physical assistant robots and their motion-based estimation," *Adv. Robot.*, vol. 29, no. 20, pp. 1315–1329, 2015, doi: 10.1080/01691864.2015.1055799.

[58] D. Shi, W. Zhang, W. Zhang, and X. Ding, "A review on lower limb rehabilitation exoskeleton robots," *Chin. J. Mech. Eng. (Engl. Ed.)*, vol. 32, no. 1, 2019. doi: 10.1186/s10033-019-0389-8.

[59] J. K. Burgess, G. C. Weibel, and D. A. Brown, "Overground walking speed changes when subjected to body weight support conditions for nonimpaired and post stroke individuals," *J. NeuroEng. Rehabil.*, vol. 7, no. 1, p. 6, 2010. doi: 10.1186/1743-0003-7-6.

[60] I. Díaz, J. J. Gil, and E. Sánchez, "Lower-limb robotic rehabilitation: Literature review and challenges," *J. Robot.*, vol. 2011, Art. ID 759764, 2011. doi: 10.1155/2011/759764.

[61] I. M. Dávila Castrodad, T. M. Recai, M. M. Abraham, J. I. Etcheson, N. S. Mohamed, A. Edalatpour, and R. E. Delanois, "Rehabilitation protocols following total knee arthroplasty: A review of study designs and outcome measures," *Ann. Transl. Med.*, vol. 7, no. Suppl. 7, p. S255, Oct. 2019. doi: 10.21037/atm.2019.08.15.

[62] J. Zhang, P. Fiers, K. A. Witte, R. W. Jackson, K. L. Poggensee, C. G. Atkeson, and S. H. Collins, "Human-in-the-loop optimization of exoskeleton assistance during walking," *Science*, vol. 356, no. 6344, pp. 1280–1284, Jun. 2017. doi: 10.1126/science.aal5054.